THE JOURNAL OF PHYSICAL CHEMISTRY C

Article

pubs.acs.org/JPCC

# Hybrid Multilayered Plasmonic Nanostars for Coherent Random Lasing

Battulga Munkhbat,[†] Johannes Ziegler,[†] Hannes Pöhl,[†] Christian Wörister,[†] Dmitry Sivun,[†] Markus C. Scharber,[‡] Thomas A. Klar,[†] and Calin Hrelescu*[,†]

[†]Institute of Applied Physics, and [‡]Linz Institute for Organic Solar Cells/Institute of Physical Chemistry, Johannes Kepler University Linz, 4040 Linz, Austria

Supporting Information

**ABSTRACT:** Here, we report that hybrid multilayered plasmonic nanostars can be universally used as feedback agents for coherent random lasing in polar or nonpolar solutions containing gain material. We show that silver-enhancement of gold nanostars reduces the pumping threshold for coherent random lasing substantially for both a typical dye (R6G) and a typical fluorescent polymer (MEH-PPV). Further, we reveal that the lasing intensity and pumping threshold of random lasers based on silver-enhanced gold nanostars are not influenced by the silica coating, in contrast to gold nanostar-based random lasers, where silica-coated gold nanostars support only amplified spontaneous emission but no coherent random lasing.

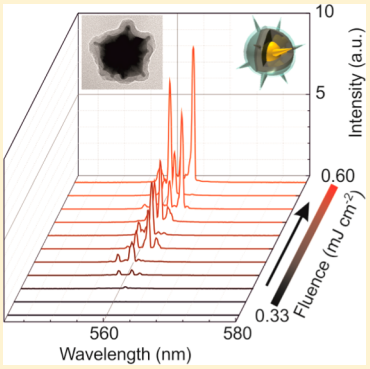


## 1. INTRODUCTION

Triggered by initial reports on lasers with mirrorless feedback,[1,2] random lasers with noncoherent (which essentially is amplified spontaneous emission, ASE)[1−4] and coherent feedback[5−7] moved closer in the focus of extensive research activities.[8,9] Coherent light amplification using high refractive index dielectric or metallic nanostructures inside a gain medium can be seen as a promising alternative to conventional lasers. While a conventional laser requires accurate fabrication and extremely precise alignment of the resonator, the resonator in a coherent random laser is realized by randomly distributed scattering nanoparticles forming closed-loops for photons.[10−12] This permits a cheap and easy fabrication method, making coherent random lasers an attractive alternative to conventional lasers in a manifold of potential applications, ranging from smart sensors and medical diagnostics,[13−16] to lighting devices[9] and displays.[17]

Noble metal nanoparticles exhibiting localized plasmon resonances[18] provide two beneficial features for coherent random lasers: much higher scattering cross sections than dielectric nanoparticles[19,20] and high field enhancements close to their surface, associated with localized plasmons.[18,21] It turns out that star-shaped gold nanoparticles, so-called gold nanostars, outperform conventionally shaped gold nanoparticles such as spheres and rods in terms of coherent random lasing.[22] Gold nanostars exhibit multiple plasmon resonances in the red and near-infrared spectral region.[23−26] These plasmon resonances associated with the tips of the gold nanostars lead to large and spectrally broad-band scattering cross sections as well as extremely strong field enhancements localized at the tips,[23−26] key features for coherent random lasers.

However, despite all of the efforts on plasmon-mediated coherent random lasing,[27−33] there are no reports on hybrid multilayered plasmonic nanostars-based coherent random lasing.

Here, we report on the development of hybrid multilayered plasmonic nanostars, which can be mixed with gain materials dissolved in either polar or nonpolar solvents. Two different, but in terms of optical properties similar, gain materials, a dye molecule and a light-emitting polymer, were dispersed in polar or nonpolar solvents, respectively. For extremely low pumping thresholds, the solutions containing gain material and silver-enhanced and silica-coated nanostars exhibit spectrally narrow lasing modes, typical for coherent random lasing. Further, we show that silver-enhancement of the gold nanostars reduces the pumping threshold for nanostar-based random lasing. Additionally, we reveal that the silica coating nearly does not influence the operation of the silver-enhanced gold nanostar-based random lasers in terms of lasing intensity and pumping threshold, in contrast to gold nanostar-based random lasers, where only ASE and no coherent random lasing was observed for the silica-coated gold nanostars.

## 2. EXPERIMENTAL SECTION

**2.1. Materials.** Silver nitrate ($AgNO_3$, 99.9999%), gold(III) chloride trihydrate ($HAuCl_4{\cdot}3H_2O$), L-ascorbic acid (AA), tetraethyl orthosilicate (TEOS), trisodium citrate dihydrate, 1

**Received:** June 7, 2016
**Revised:** October 1, 2016
**Published:** October 4, 2016




DOI: 10.1021/acs.jpcc.6b05737
J. Phys. Chem. C 2016, 120, 23707−23715

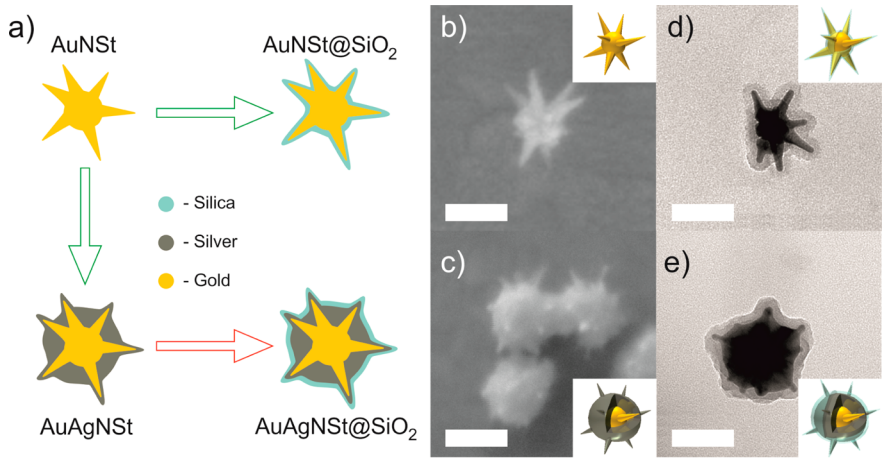


**Figure 1.** (a) Sketch of the synthesis route for hybrid multilayered nanostars. SEM images of a representative (b) AuNSt and of representative (c) AuAgNSts. TEM images of a representative (d) AuNSt@$SiO_2$ and (e) AuAgNSt@$SiO_2$. The scale bars are 100 nm. Insets: Schematics of the corresponding nanostars illustrating the layered composition.

N hydrochloric acid solution (HCl), sodium borohydride ($NaBH_4$, 99%), hexadecyltrimethylammonium bromide (CTAB), *O*-[2-(3-mercaptopropionylamino)ethyl]-*O*′-methylpoly(ethylene glycol) (mPEG-SH, MW 5K), ammonium hydroxide ($NH_4OH$, 30%), and Rhodamine 6G (R6G) were purchased from Sigma-Aldrich at the highest purity grade available. Commercial poly[2-methoxy-5-(2-ethylhexyloxy)-1,4-phenylene-vinylene] end-capped with polysilsesquioxane (ADS200RE, purchased from American Dye Source) was used without further purification. Citrate-capped spherical gold nanoparticles (125 nm in diameter) were purchased from Nanopartz. Carbon-coated copper TEM grids were purchased from Plano GmbH. Ethanol absolute (99.9%) was purchased from Fisher Chemical. All glassware and stir bars were thoroughly cleaned with aqua regia and dried prior to use. Ultrapure distilled water (Millipore, 18 MΩ cm) was used in all steps of nanoparticle preparation.

**2.2. Synthesis of Hybrid Multilayered Plasmonic Nanostars.** The hybrid multilayered plasmonic nanostars were synthesized according to the synthesis route in Figure 1a. First, gold nanostars (AuNSts) functionalized with CTAB were synthesized. Subsequently, aliquots from the same solution containing freshly synthesized AuNSts were branched off for further coating of the AuNSts, either for coating with a silver shell for plain silver-enhancement (AuAgNSts), for silver-enhancement and subsequent coating with a thin silica shell (AuAgNSts@$SiO_2$), or for coating with a thin silica shell only (AuNSts@$SiO_2$). To avoid aggregation and to improve the stability of the nanostars without silica shell dispersed in ethanol, the CTAB was replaced with thiolated mPEG (mPEG-SH) in case of the AuNSts and AuAgNSts via a ligand exchange reaction.

*2.2.1. Synthesis of Gold Nanostars.* For the synthesis of the gold nanostars (AuNSts), we modified a previously reported seed-mediated method in aqueous solution.[22,34] Sodium citrate-functionalized gold nanoparticles of 3−5 nm in diameter were used as seeds for the growth of the AuNSts. The gold seed particles were prepared by adding 0.6 mL of ice cold 0.1 M $NaBH_4$ to a 20 mL aqueous solution containing 0.25 mM $HAuCl_4$ and 0.25 mM sodium citrate under vigorous stirring.[35] The solution was kept stirring for 3 h at room temperature. For the growth of AuNSts, 100 μL of the aged seed solution was added to 10 mL of an aqueous solution of 0.25 mM gold chloride ($HAuCl_4$), hereafter called growth solution. The pH was adjusted by adding 10 μL of 1 N hydrochloric acid (HCl). Subsequently, 100 μL of 2 mM silver nitrate ($AgNO_3$) and 50 μL of 0.1 M ascorbic acid (AA) were simultaneously added to the growth solution under vigorous stirring. The nanostars were functionalized with hexadecyltrimethylammonium bromide (CTAB); that is, 100 μL of 0.1 M CTAB was added to the growth solution, which was left stirring for 5 min. The solutions containing AuNSts were washed by centrifugation (2000 rcf for 20 min), and redispersed in a 10 mL of 1 mM aqueous CTAB solution. Figure 1a shows the SEM image of a representative AuNSt. The scale bar is 100 nm. More exemplary SEM images are shown in Figure S1. Such AuNSts with long and sharp tips, pointing in arbitrary directions, exhibit multiple plasmon resonances, strong field enhancements located at their tips, as well as large scattering cross sections.[26]

*2.2.2. Synthesis of Silver-Enhanced Gold Nanostars.* For the silver-enhanced gold nanostars (AuAgNSts), we followed a method that was inspired by the method reported by Fales et al.[36] 5 μL of 0.1 M $AgNO_3$ and an equivalent volume of 0.1 M AA were added as a precursor and as a reducing agent, respectively, under vigorous stirring to 1 mL of CTAB-functionalized AuNSts in solution. After 15 min, the silver enhanced gold nanostars were purified by centrifugation at 2000 rcf for 10 min, discarding the supernatant, and redispersed in 1 mL of distilled water. Figure 1b shows an SEM image of representative AuAgNSts. The AuAgNSts still exhibit sharp tips, but the branch length of the previously long gold nanostar tips protruding from the core of the nanostars is reduced while the core diameter is increased due to the silver-enhancement. Several examples of SEM images can be found in Figure S2. The exact silver shell thickness of the AuAgNSts can hardly be measured precisely with a TEM, due to the limited material contrast. However, we can distinguish between the gold nanostar and the silver shell in high angle annular dark field TEM images, so that we estimate the silver shell thickness to be in the range of 20 nm around the core of the gold nanostar (an example is shown in Figure S3). Further, from elemental line and mapping analysis of representative AuAgNSts using energy dispersive X-ray spectroscopy (EDX), we assume that the apexes of the tips are also covered by a very thin (<8 nm) silver shell (Figure S3). The presented synthesis methods for the AuNSts and AuAgNSts allow a high reproducibility with


DOI: 10.1021/acs.jpcc.6b05737
J. Phys. Chem. C 2016, 120, 23707−23715

negligible batch-to-batch variations in the optical ensemble spectra (Figure S4).

*2.2.3. Silica Coating of the AuNSts and AuAgNSts.* To obtain a homogeneous and thin (<10 nm) silica shell that follows the morphology of the nanostars, the original recipe,[37] which provides substantially thicker shells, had to be modified. The freshly synthesized and washed AuNSts and AuAgNSts were functionalized with thiolated mPEG (mPEG-SH) via a ligand exchange reaction. mPEG-SH was mixed with 1 mL of aqueous solution containing nanostars to a final concentration of 5 $\mu$M under gentle stirring for 1 h. The PEGylated nanostars were washed once more by centrifugation (2500 rcf for 10 min) to remove the residual ligands and were redispersed in a mixed solution of ethanol (0.9 mL) and water (0.2 mL). Under gentle stirring, silica (TEOS) coating of the nanostars was initiated by adding 10 $\mu$L of $NH_4OH$ followed by 3 $\mu$L of 10% TEOS in ethanol. The reaction was allowed to proceed for 12 h. After that, the nanostars were washed three times by centrifugation at 3000 rcf for 5 min and redispersed in ethanol or chlorobenzene. In Figure 1c and d, TEM images of representative silica-coated nanostars, AuNSt@$SiO_2$ and AuAgNSt@$SiO_2$, are shown (see Figures S5 and S6 for more examples of AuNSt@$SiO_2$ and AuAgNSt@$SiO_2$, respectively). The average silica shell thickness was about 10 nm based on TEM image analysis of several nanoparticles (Figure S7). In both cases, the shell was uniformly and completely formed around the nanostars, maintaining their morphology. As a major benefit, this thin silica shell allows mixing of both nanostar types, AuNSts@$SiO_2$ and AuAgNSts@$SiO_2$, with polar (ethanol) as well as nonpolar organic solvents (chlorobenzene) without causing aggregation. In addition, the silica shell of around 10 nm is thick enough to prevent chemical degradation such as oxidation of silver in the case of AuAgNSts@$SiO_2$. It is worth rementioning that all of the displayed nanostars stem from the same original batch of gold nanostars. For a period of 10 h without stirring, no precipitation or aggregation of the nanostars was observed. Figure S8 shows the corresponding extinction spectra of AuAgNSts with and without silica shell dispersed in ethanol recorded every hour for 10 h. All nanostars have similar tip-to-tip diameters of about 100−150 nm (the corresponding histograms can be found in Figure S9). For reference, citrate-functionalized spherical nanoparticles (AuNPs) with diameters of about 120 nm were also coated with silica using the same procedure as for the nanostars (examples of SEM and TEM images of AuNPs and AuNPs@$SiO_2$ are displayed in Figure S10).

**2.3. Characterization Methods.** Extinction spectra were measured by a Varian Cary 500 Scan UV−vis−NIR spectrophotometer. For the characterization of the morphology, solutions containing AuNSts and AuAgNSts were drop casted on cleaned ITO substrates, dried, and analyzed with a Zeiss Smart SEM Supra 55 VP scanning electron microscope (SEM). For the transmission electron microscope (TEM) characterization, solutions containing silica-coated AuAgNSts and AuNSts were drop casted on carbon-coated copper TEM grids, dried, and analyzed using a JEOL JEM-2010 TEM.

Scanning TEM (STEM) was performed with bright field (BF) and high angle annular dark field (HAADF) detectors. Elemental line and mapping analyses were carried out using energy dispersive X-ray spectroscopy (EDX). The samples were investigated with a JEOL JEM-2200FS transmission electron microscope in STEM mode operated at 200 kV, equipped with an Oxford SDD X-maxN (80 $mm^2$) EDX-system.

**2.4. Gain-Nanostar Solutions.** For preparation of the randomly lasing systems, Rhodamine 6G (R6G) and ADS200RE (a MEH-PPV derivate) were used without further treatment. R6G (2 mg $mL^{-1}$) or MEH-PPV (7 mg $mL^{-1}$) dissolved in ethanol or chlorobenzene, respectively, were used as stock solutions. In the following, we refer to the R6G dissolved in ethanol as to the R6G solution and to the ADS200RE dissolved in chlorobenzene as to the MEH-PPV solution. The nanoparticle concentrations were controlled by gentle centrifugation and redispersion in ethanol or chlorobenzene. AuNSts and AuNSts@$SiO_2$ in ethanol exhibit the same optical density (OD) at 405 nm (d-band absorption of gold). The AuAgNSts and AuAgNSts@$SiO_2$ were directly synthesized out of a part of the AuNSts, so that the concentrations are considered to be similar. The corresponding extinction spectra are shown in Figure S11. Because all four types of the nanostars can be dispersed in ethanol without aggregation, 0.3 mL of each type of the nanostars dispersed in ethanol was mixed with 1 mL of the R6G solution. As a reference without any nanoparticles, 0.3 mL of ethanol was mixed with 1 mL of R6G solution. In the case of the MEH-PPV solutions, either 0.3 mL of AuNSts@$SiO_2$, or 0.3 mL of AuAgNSts@$SiO_2$ or silica-coated spherical nanoparticles (AuNPs@$SiO_2$) dispersed in chlorobenzene was mixed with 1 mL of MEH-PPV solution. The concentration of AuNP@$SiO_2$ dispersion was adjusted in such a way that its OD at 405 nm (d-band absorption of gold) was the same as the OD of the AuNSt@$SiO_2$ dispersion (Figure S11c). As reference mixture of MEH-PPV without any nanoparticles, 0.3 mL of chlorobenzene was mixed with 1 mL of MEH-PPV solution. The final mixtures contain similar concentrations of nanostars/nanoparticles and either R6G (1.5 mg $mL^{-1}$) or MEH-PPV (5.4 mg $mL^{-1}$). For more clarity, we denote each suspension as nanostar type/gain material, for example, AuNSt/R6G.

**2.5. Random Lasing Experiments.** For random lasing experiments, quartz cuvettes with four transparent windows (inner dimensions 10 mm × 4 mm) containing 0.5 mL of the solutions were used as containers. We used a setup, which basically resembles the variable stripe length method[38] for cuvettes, that is, a stripe-like excitation illumination of the cuvette through the 10 mm window. The detection through the 4 mm side window was almost perpendicular to the excitation. To avoid possible Fabry−Perot feedback between the cuvette inner walls, the cuvette was slightly tilted with respect to the direction of the excitation stripe. Thus, any signals stemming from multiple reflections are not fed into the detector. Figure 2 shows the excitation and detection scheme for the random lasing experiments. A diode-pumped, passively Q-switched solid state laser (CryLas GmbH, pulse length shorter than 1.3 ns, maximal pulse energy 20 $\mu$J) was used to excite the suspensions at a wavelength of 532 nm. Single pulse excitation was used to prevent photobleaching of the gain medium. The excitation beam was shaped into a thin stripe by two crossed cylindrical lenses and focused in the plane of two razor blades. To establish a 3 mm long, 55 $\mu$m wide excitation stripe on the suspensions in the cuvette, the homogeneous central part of the beam is selected by the razor blades. The emission from the pumped excitation volume was coupled out of the side window and focused onto the entrance slit of the spectrometer (Newport MS260i), which was equipped with a Peltier-cooled charge-coupled device camera (Andor iVac). A 532 nm notch filter was used to suppress detection of scattered excitation light. To quantitatively compare the random lasing from the



DOI: 10.1021/acs.jpcc.6b05737
J. Phys. Chem. C 2016, 120, 23707−23715

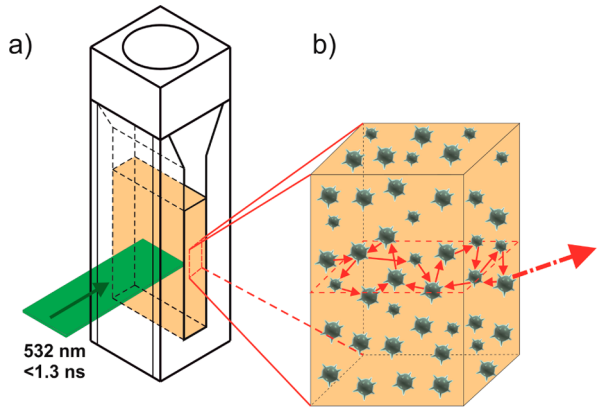


**Figure 2.** (a) Illustration of the excitation stripe and the detection of the emission. (b) The nanostars can randomly form resonant cavities in the gain medium and hence the necessary feedback mechanism for random lasing.

different gain-nanostar solutions, all measurements were performed under exactly the same experimental conditions. In all random lasing experiments, the size of the excitation stripe, the position of the cuvette in the setup, the position of the excitation stripe on the cuvette's window, and the integration time (1 s) for the detection were fixed.

## 3. RESULTS

### 3.1. Nanostars as Resonators in Ethanol Solutions.

Figure 3a displays the absorption (Abs) and photoluminescence (PL) spectra of R6G dispersed in ethanol. The dashed orange curve in Figure 3b zooms into the PL spectrum of R6G from 545 to 580 nm, taken at a pumping fluence of 0.24 mJ $cm^{-2}$. For this fluence, the PL intensity was magnified 30 times to be visible on the scale of the ordinate in Figure 3b. For fluences above 0.30 mJ $cm^{-2}$, the emission spectrum of the reference R6G solution shows amplified spontaneous emission (ASE) with a substantially reduced spectral bandwidth as compared to PL (see Figure S12). The curves shaded from black to red in Figure 3b show the ASE spectra of the reference R6G solution without nanostars excited by single pulses at different excitations fluences, ranging from 0.33 to 0.66 mJ $cm^{-2}$, increasing with equal steps of 0.03 mJ $cm^{-2}$.

AuNSts dispersed in ethanol exhibit a spectrally broad extinction spectrum with a maximum around 630 nm, due to the multiple plasmon resonances of each individual nanostar (Figure 3c, blue curve). The plasmon resonances of the AuNSts

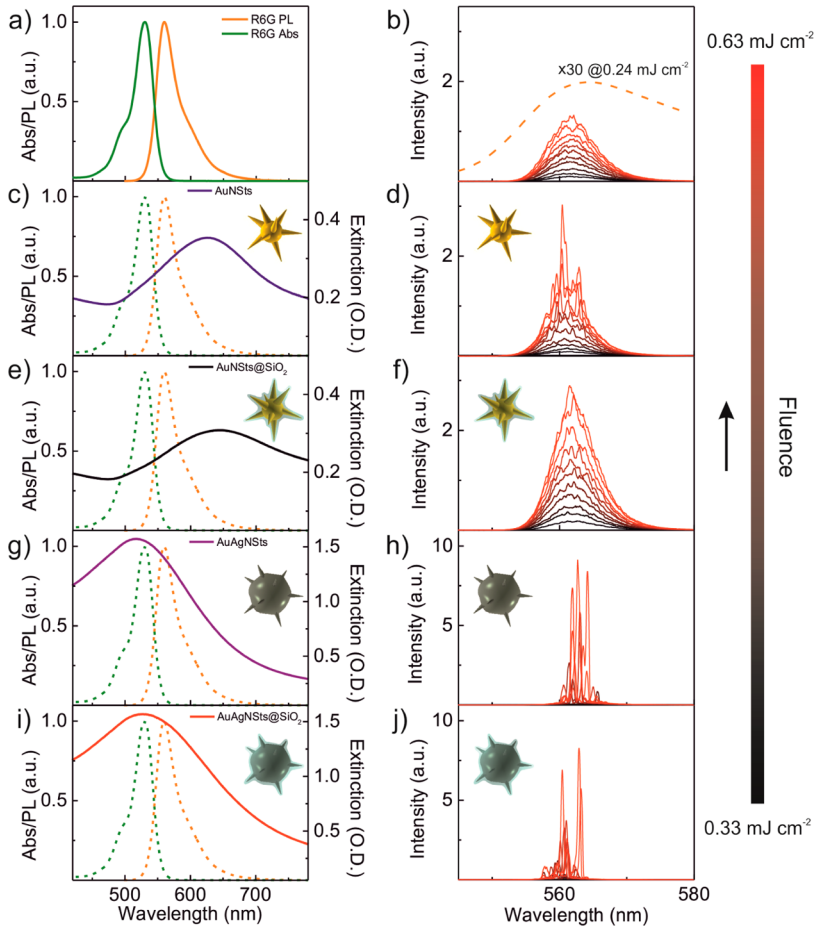


**Figure 3.** (a) Normalized absorption (green) and photoluminescence (PL) (orange) spectra of R6G; (b) ASE spectra of the reference R6G solution without nanostars, excited by single pulses at different excitation fluences from 0.33 to 0.66 mJ $cm^{-2}$ in steps of 0.03 mJ $cm^{-2}$. The intensity of the PL spectra of R6G at a pumping fluence of 0.24 mJ $cm^{-2}$ (dashed orange curve) was magnified 30 times for comparison. (c,e,g,i) Spectral overlap of the R6G absorption and emission spectra (dotted curves) with the extinction spectra of respective nanostars in ethanol (solid lines) and (d,f,h,j) the emission (random lasing or ASE) spectra at different excitations fluences for nanostars/R6G mixtures. (c,d) AuNSts, (e,f) AuNSts@$SiO_2$, (g,h) AuAgNSts, and (i,j) AuAgNSts@$SiO_2$, respectively.



DOI: 10.1021/acs.jpcc.6b05737
J. Phys. Chem. C 2016, 120, 23707−23715

spectrally overlap partially with the PL emission of R6G (dashed orange curve in Figure 3c), but they hardly overlap with the R6G absorption. At lower pumping fluences, ASE is observed from the AuNSt/R6G sample (Figure 3d), similar to the ASE of the R6G reference (Figure 3b). For higher fluences, sharper features are emerging out of the ASE background. This behavior is typical for random lasers: ordinary PL is observed for low pumping fluences, ASE is observed for a fairly broad range of pumping fluences, followed by coherent laser peaks for even higher pumping fluences.

Upon silica-coating, the plasmon resonances of the AuNSts red-shift by about 20 nm due to the introduction of a higher refractive index medium around the AuNSts as compared to the solvent (see Figure 3e). To underline our findings, we performed three-dimensional finite difference time domain (FDTD) calculations on the optical properties of the hybrid multilayered nanostars. The calculated plasmon resonance of a single AuNSt with silica shell is red-shifted as compared to the plasmon resonance of the same single AuNSt without the silica shell (Figure S14). For a detailed description of the numerical calculation on the plasmonic properties of hybrid multilayered plasmonic nanostars, refer to the corresponding section in the Supporting Information.

Surprisingly, the AuNSt@$SiO_2$/R6G sample exhibits only pronounced ASE even at the highest pumping fluence (Figure 3f). The silica shell affects the gold nanostar-based random lasers in several ways. First, the local field enhancements at the surface of the AuNSts@$SiO_2$ are slightly reduced by the silica coating. The maximal field intensity is localized close to the gold tip in the silica shell (see Figure S15), so that outside the silica shell the efficient excitation of the nearby gain material might also be reduced. Second, besides the spectral red-shift, the silica shell induces a spectral broadening of the plasmon resonances, typically for chemical damping of the plasmon resonances,[18] leading to a small reduction in the spectral overlap between the PL of R6G and the plasmon resonances of the AuNSts@$SiO_2$. Third, the silica shell acts as a spacer between the gain material and the gold reducing quenching. While the latter is beneficial for random lasing, the small reduction in the spectral overlap between AuNSts@$SiO_2$ scattering and the PL of R6G as well as slight reduction of the field enhancements possibly diminish the feedback for coherent random lasing.

The silver-enhancement of the AuNSts leads to a blue-shift of the plasmon resonances from around 630 nm (AuNSts, Figure 3b) down to 530 nm (AuAgNSts, Figure 3g). Hence, the extinction spectra of the AuAgNSts in ethanol spectrally overlap with both the absorption and the PL of the R6G. The blue-shift of the plasmon resonances can be attributed to a mixed gold−silver dielectric function,[39] as well as to the reduced length of the nanostars' tips protruding from the core and to an increased diameter of the core induced by the silver-enhancement[36] (see Figures S14 and S16). Additionally, due to the high scattering efficiency of silver, the AuAgNSts in ethanol exhibit ∼4 times higher extinction as compared to the AuNSts (note the different scales of the ordinate in Figure 3b and g), although the concentrations of the nanostars were similar in both dispersions.

Spectrally very sharp and intense random lasing peaks, characteristic for coherent random lasing, are observed for the AuAgNSt/R6G sample. Surprisingly, no pronounced ASE background is detected even at low pumping fluences (Figure 3h and Figure S13), in contrast to the previously mentioned samples. The investigation of the underlying physical mechanisms for this experimental observation is beyond the scope of this Article. The maximally observed random lasing intensities are more than 3-fold higher than the random lasing intensities detected from the AuNSt/R6G.

Silica coating of the AuAgNSts leads to a spectral red-shift (20 nm) of the plasmon resonances, so that the extinction spectra of the AuAgNSts@$SiO_2$ in ethanol perfectly overlap with the absorption and the PL of the R6G (Figure 3i). No sign of a possible detrimental effect of the silica coating on the random lasing characteristics was observed in the case of the AuAgNSt@$SiO_2$/R6G sample (Figure 3j), in contrast to the AuNSt@$SiO_2$/R6G case (Figure 3f). Moreover, the random lasing intensities are comparable for both samples. As for the AuAgNSt/R6G sample, coherent random lasing is observed also for the AuAgNSt@$SiO_2$/R6G sample even at low pumping fluences (Figure 3j).

For the sake of better visualization, the random lasing spectra of the AuAgNSt/R6G and AuAgNSt@$SiO_2$/R6G from Figure 3h and j are redisplayed in Figure 4a and b, respectively. For

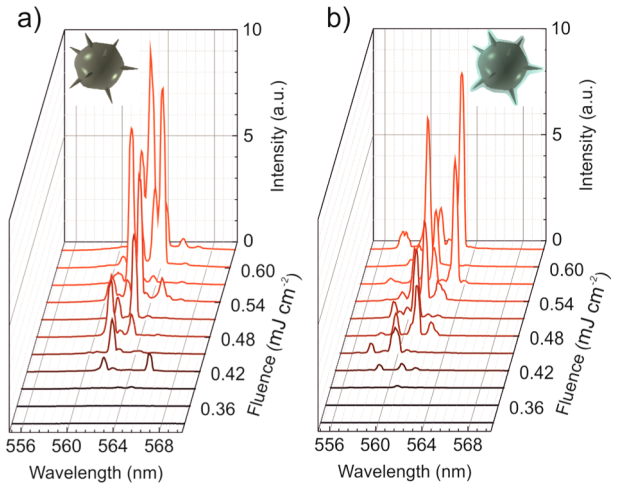


**Figure 4.** Random lasing spectra of the (a) AuAgNSt/R6G and (b) AuAgNSt@$SiO_2$/R6G samples excited by single pulses at different excitation fluences.

both samples, the measured spectral width of the coherent random lasing peaks is as small as 0.3 nm, corresponding to the resolution of the spectrometer. Hence, the values represent an upper limit, while the actual line widths of the lasing modes might be well below. The spectral position, number, and relative intensities of the random lasing peaks vary from pulse to pulse. The closed loop resonator cavities of the random laser, formed by the nanostars, change from shot to shot, due to Brownian motion. There are several effects that can contribute to the fact that the AuAgNSts as well as the AuAgNSts@$SiO_2$ could facilitate the buildup of coherent lasing modes. First, the plasmon resonances of the AuAgNSts and AuAgNSts@$SiO_2$ spectrally overlap with both the absorption and the emission of R6G in ethanol, in contrast to AuNSts. Second, the stronger hot spots at the tips of the AuAgNSts or AuAgNSts@$SiO_2$ as compared to hot spots at the tips of the AuNSts (see Figure S15) might provide a more efficient pumping of the gain material, promoting inversion. Third, the AuAgNSts could provide coherent feedback for random lasing at ∼560 nm, due to their high scattering cross sections in the spectral region


DOI: 10.1021/acs.jpcc.6b05737
J. Phys. Chem. C 2016, 120, 23707−23715

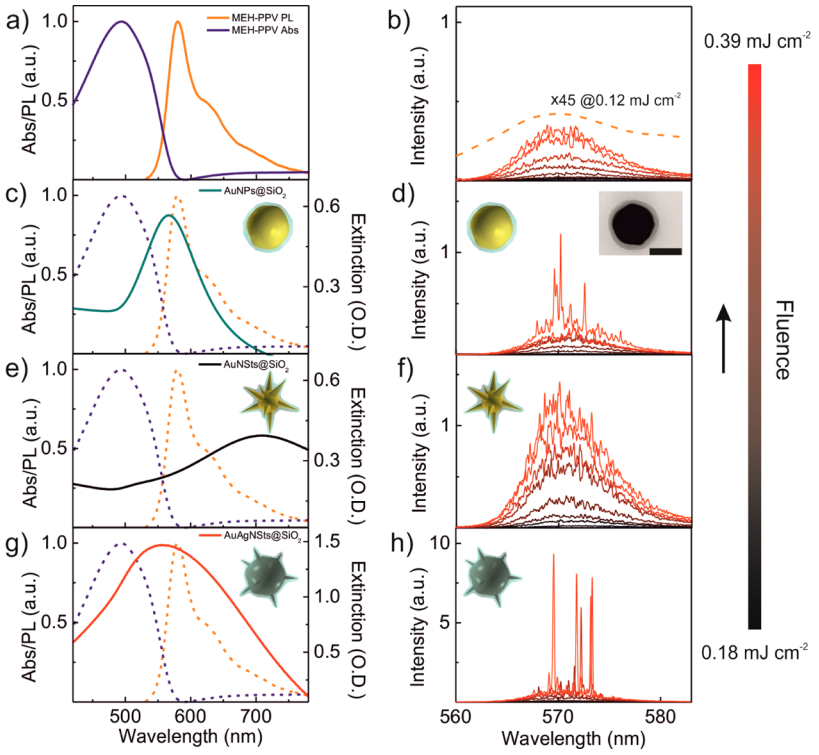


**Figure 5.** (a) Normalized absorption (blue) and photoluminescence (PL) (orange) spectra of the MEH-PPV in chlorobenzene solution; (b) ASE spectra of the reference MEH-PPV solution without nanostars, excited by single pulses at different excitation fluences. The intensity of the PL spectra of MEH-PPV at a pumping fluence of 0.12 mJ $cm^{-2}$ (dashed orange curve) was magnified 45 times for comparison. (c–h) Spectral overlap of the MEH-PPV absorption and emission spectra (dotted curves) with the extinction spectra of respective silica-coated nanoparticles in chlorobenzene (solid lines) and the emission (ASE or random lasing) spectra at different excitations fluences for nanoparticles/MEH-PPV mixtures: (c,d) AuNPs@$SiO_2$, (e,f) AuNSts@$SiO_2$, (g,h) AuAgNSts@$SiO_2$, respectively. The inset in (d) shows the TEM image of a representative AuNP@$SiO_2$ nanoparticle. The scale bar is 100 nm.

coinciding to the spectral position of the main PL maximum of R6G (560 nm) (see Figure S14).

**3.2. Nanostars as Resonators in Chlorobenzene Solutions.** Next, we show that silica-overcoated nanostars can not only be used as scatterers for random lasing in the polar solvent ethanol, but also in the nonpolar solvent chlorobenzene. The normalized absorption and PL spectra of MEH-PPV dissolved in chlorobenzene are displayed in Figure 5a. Figure 5b shows the ASE spectra of the reference MEH-PPV solution without nanostars excited by single pulses at different excitation fluences, ranging from 0.18 to 0.39 mJ $cm^{-2}$ increasing with equal steps of 0.03 mJ $cm^{-2}$. In the case of the MEH-PPV reference sample and for small excitations fluences (<0.18 mJ $cm^{-2}$), one observes PL only. The dashed orange curve in Figure 5b shows the PL spectra of MEH-PPV at a pumping fluence of 0.12 mJ $cm^{-2}$. The PL intensity was magnified 45 times for comparison with ASE. For excitation fluences above 0.18 mJ $cm^{-2}$, the MEH-PPV reference sample shows ASE (see Figure S17).

As a further reference, spherical nanoparticles with dimension similar to that of the nanostars (125 nm in diameter) and coated with a 10 nm silica shell (AuNPs@$SiO_2$) were used to prepare AuNP@$SiO_2$/MEH-PPV samples. The plasmon resonances of the AuNPs@$SiO_2$ in chlorobenzene spectrally overlap with the PL spectra of the MEH-PPV (Figure 5c). The inset in Figure 5d displays the TEM image of a representative AuNP@$SiO_2$ nanoparticle. As shown in Figure 5d, coherent random lasing arising from the ASE background could be observed for the AuNP@$SiO_2$/MEH-PPV sample only for the highest fluences.

The random lasing intensity for a pumping fluence of 0.39 mJ $cm^{-2}$ is increased by a factor of ~3 with respect to ASE intensities detected for the other pumping fluences, which are comparable to the ASE intensities observed for the reference MEH-PPV sample (Figure 5d).

The extinction spectrum of the AuNSts@$SiO_2$ dispersed in chlorobenzene (black curve) is shown in Figure 5e. The AuNSt@$SiO_2$/MEH-PPV sample exhibits prominent ASE (Figure 5f), as was previously observed also for the AuNSt@$SiO_2$/R6G sample (Figure 3f). For fluences above 0.30 mJ $cm^{-2}$, coherent random lasing peaks can be observed on top of the pronounced ASE background. It is worth mentioning that, although the plasmon resonances of the AuNSts@$SiO_2$ dispersed in chlorobenzene spectrally overlap with the second PL emission maximum of MEH-PPV (at 630 nm), no ASE or random lasing was observed from the AuNSt@$SiO_2$/MEH-PPV sample in this spectral region.

Figure 5g shows the extinction spectra of the AuAgNSts@$SiO_2$ in chlorobenzene. The plasmon resonances of the AuAgNSts@$SiO_2$ in chlorobenzene spectrally overlap with both the absorption and the PL spectra of MEH-PPV. For the AuAgNSt@$SiO_2$/MEH-PPV sample, coherent random lasing was observed starting with pumping fluences above 0.24 mJ $cm^{-2}$ (Figure 5h). In Figure S18, the random lasing spectra of the AuAgNSt@$SiO_2$/MEH-PPV sample excited by single pulses at different excitations fluences are displayed in a fashion similar to those in Figure 4.



DOI: 10.1021/acs.jpcc.6b05737
J. Phys. Chem. C 2016, 120, 23707–23715

**3.3. Comparison of Results.** For a more quantitative comparison of the different samples, we analyze the maximal emission intensity, that is, the maximal intensity of the ASE or coherent random lasing in Figure 3 and Figure 5, as a function of the applied pumping fluence for the samples containing R6G (Figure 6a) or MEH-PPV (Figure 6b) as a gain material, respectively.

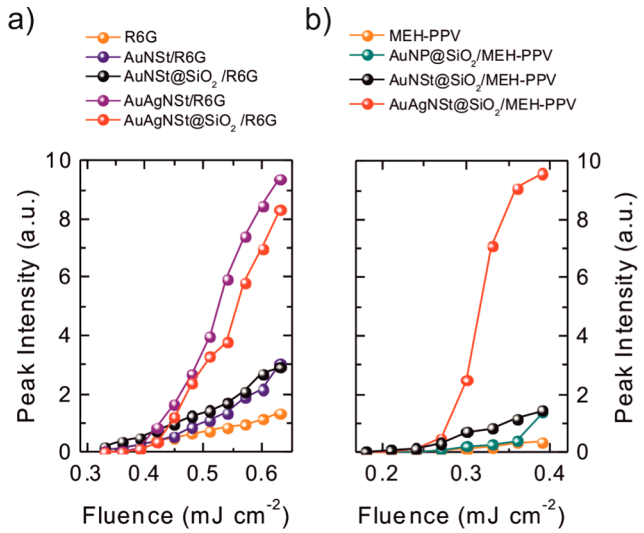


**Figure 6.** (a) Maximal emission intensities of the ASE or random lasing spectra (Figure 3) as a function of the corresponding pumping fluence for R6G reference sample without nanoparticles (orange), for AuNSt/R6G (blue), AuNSt@$SiO_2$/R6G (black), AuAgNSt/R6G (purple), and AuAgNSt@$SiO_2$/R6G samples (red). (b) Maximum emission intensities of the ASE or random lasing spectra (Figure 5) as a function of the corresponding pumping fluence for MEH-PPV reference solution (orange), for AuNP@$SiO_2$/MEH-PPV (dark cyan), AuNSt@$SiO_2$/MEH-PPV (black), and AuAgNSt@$SiO_2$/MEH-PPV (red) samples, respectively.

For the R6G reference sample without nanoparticles, the ASE intensity increases with increasing pumping fluences (the orange curve in Figure 6a). As expected from Figure 3b, there is no hint for a coherent random lasing threshold. The blue curve in Figure 6a refers to the spectra of AuNSt/R6G sample in Figure 3d. One is able to identify two distinctively different slopes of the blue curve. For low fluences (<0.45 mJ $cm^{-2}$), the AuNSt/R6G sample exhibits ASE similar to that of the R6G reference sample. At around 0.45 mJ $cm^{-2}$, the slope of the blue curve changes, indicating the coherent random lasing threshold of the AuNSt/R6G sample. The black curve in Figure 6a, depicting the maximal intensities of the spectra displayed in Figure 3h for AuNSt@$SiO_2$/R6G samples, shows a trend with increasing pumping fluences similar to that of the R6G reference sample. As one can deduct from the steeper slope of the black curve as compared to the orange curve, the AuNSts@$SiO_2$ facilitate ASE. The red and purple curves in Figure 6a correspond to the maximal random lasing intensities from the AuAgNSt/R6G (red) and AuAgNSt@$SiO_2$/R6G (purple) samples, respectively. The threshold fluences for coherent lasing are at 0.39 mJ $cm^{-2}$ (red curve) and at 0.42 mJ $cm^{-2}$ (purple curve), respectively. Saturation of peak intensities is observed for high fluences.

In the case of AuAgNSt@$SiO_2$/MEH-PPV, the threshold fluence for coherent lasing is at 0.24 mJ $cm^{-2}$, while the onset for coherent random lasing for the AuNP@$SiO_2$/MEH-PPV sample (dark cyan curve in Figure 6b) is at much higher pumping fluences (0.36 mJ $cm^{-2}$). At a fluence of 0.39 mJ $cm^{-2}$, the coherent random lasing emission intensity from the AuAgNSt@$SiO_2$/MEH-PPV sample is ~8.3 times higher than the emission intensities observed from the samples containing AuNPs@$SiO_2$ (dark cyan curve) or AuNSts@$SiO_2$ (black curve).

However, saturation of peak intensities is clearly visible in Figure 6b. Moreover, the maximal detected random lasing intensity for the AuAgNSt@$SiO_2$/MEH-PPV sample is boosted by a factor of ~25 as compared to maximal ASE intensity from the reference MEH-PPV sample (orange curve).

Our observations can be explained by the unique properties of the AuAgNSts as compared to other particles. The AuAgNSts and the AuAgNSts@$SiO_2$ exhibit higher scattering cross sections than the AuNPs@$SiO_2$ and the AuNSts with and without silica shell, due to the silver-enhancement. The higher scattering cross section might be one of the main reasons for the low pumping thresholds at which the solutions containing AuAgNSts or AuAgNSts@$SiO_2$ show coherent random lasing. Another reason could be the spectral overlap of the plasmon resonances with the absorption spectra of the gain material and the excitation wavelength. The hot-spots at the tips of the AuAgNSts could facilitate the creation of inversion by providing more efficient pumping of the gain material. Similar correlations between the lasing thresholds and the field enhancement were reported also by others.[40]

Finally, we turn our discussion to the comparison of pumping thresholds for the AuAgNSt@$SiO_2$/R6G and AuAgNSt@$SiO_2$/MEH-PPV-based random lasers. Because the concentrations of AuAgNSts@$SiO_2$ in the R6G and MEH-PPV solutions were the same, we analyze the lasing thresholds with respect to the extinction $A = \varepsilon cd$ of the gain materials in the stock solutions. $\varepsilon$ is the extinction coefficient of R6G (219 mL $mg^{-1}$ $cm^{-1}$ taken from ref 41) or MEH-PPV (106 mL $mg^{-1}$ $cm^{-1}$ from ref 42 assuming that $\varepsilon$ of MEH-PPV in chlorobenzene is in the same order of magnitude as in chloroform), $c$ is the concentration of the gain materials, and $d$ is the optical path of 4 mm. The extinction of the AuAgNSt@$SiO_2$/R6G solutions ($c$ = 1.5 mg $mL^{-1}$) is $A_{R6G} \approx 132$, while the AuAgNSt@$SiO_2$/MEH-PPV solutions (5.4 mg $mL^{-1}$) have an extinction $A_{MEH-PPV} \approx\sim 229$. For the AuAgNSt@$SiO_2$/MEH-PPV sample, coherent random lasing without pronounced ASE background was observed starting with pumping fluences above 0.24 mJ $cm^{-2}$. Considering that $A_{MEH-PPV} \approx 1.73\ A_{R6G}$, the lasing threshold for the AuAgNSt@$SiO_2$/R6G should be ~1.73 higher than the lasing threshold for AuAgNSt@$SiO_2$/MEH-PPV. Indeed, the experimental threshold for coherent random lasing of AuAgNSt@$SiO_2$/R6G (0.42 mJ $cm^{-2}$) is 1.75 times higher than the threshold for AuAgNSt@$SiO_2$/MEH-PPV.

## 4. CONCLUSION

In summary, we synthesized hybrid multilayered plasmonic nanostars, comprised of gold, silver, and silica in various compositions. The silver-enhanced and silica-coated gold nanostars can be mixed with polar or nonpolar solutions containing gain material. We find that AuAgNSts and AuAgNSts@$SiO_2$ provide sufficient feedback for coherent random lasing. In single pulse experiments, we show that the silver-enhancement of the gold nanostars reduces the pumping threshold for nanostar-based coherent random lasers substantially in different gain media. We attribute this to the plasmon


DOI: 10.1021/acs.jpcc.6b05737
J. Phys. Chem. C 2016, 120, 23707−23715

resonances of AuAgNSts and AuAgNSts@$SiO_2$, which spectrally overlap perfectly with both the absorption and PL emission of the gain materials as well as the excitation wavelength. Several effects probably work together to facilitate random lasing with low pumping fluences. First, hot-spots at the tips of the AuAgNSts and of AuAgNSts@$SiO_2$ can be resonantly excited by the pumping laser, and hence the gain material in the vicinity of the tips can be excited with a higher effective intensity. Therefore, the AuAgNSts and AuAgNSts@$SiO_2$ can facilitate inversion of the gain material more easily. Second, the AuAgNSts and the AuAgNSts@$SiO_2$ can provide the necessary feedback for coherent. Considering the perfect spectral overlap of the plasmon resonances with the PL of the gain material and the high scattering cross sections of the AuAgNSts and AuAgNSts@$SiO_2$, the emitted photons can be scattered efficiently. Further, we reveal that the lasing intensity and pumping threshold of a silver-enhanced gold nanostar-based random laser are basically not influenced by the silica coating, in contrast to the gold nanostar-based random laser, where for the silica-coated gold nanostars only mediate ASE but no coherent random lasing was observed.

The large scattering cross sections and easily accessible hot-spots provided by AuAgNSts and the simultaneous compatibility of the AuAgNSts@$SiO_2$ with polar and nonpolar solvents render hybrid multilayered plasmonic nanostars one of the most promising candidates for an effective photon-management in organic and inorganic optoelectronic devices as well as for biosensing and analytical applications.

## ■ ASSOCIATED CONTENT

### Supporting Information

The Supporting Information is available free of charge on the ACS Publications website at DOI: 10.1021/acs.jpcc.6b05737.

Additional extinction spectra, SEM, TEM images, EDX elemental maps of the AuAgNSts, and numerical modeling of hybrid multilayered plasmonic nanostars, as well as the random lasing spectra of the AuAgNSt@$SiO_2$/MEH-PPV sample displayed in a fashion similar to Figure 4 (PDF)

## ■ AUTHOR INFORMATION


### Corresponding Author

*Phone: +43 732 2468 9240. E-mail: calin.hrelescu@jku.at.


### Notes

The authors declare no competing financial interest.

## ■ ACKNOWLEDGMENTS

We would like to cordially thank Heidi Piglmayer-Brezina and Wolfgang Grafeneder for taking the SEM and TEM images and Heiko Groiß for performing EDX elemental mapping and taking the STEM images. We acknowledge financial support by the European Research Council (ERC Starting Grant 257158 "Active NP") and by the Austrian Klima- und Energiefonds (SolarTrap, Grant 843929) in the framework of "Energy Mission Austria". B.M. acknowledges financial support by the Erasmus Mundus Mobility Project GATE.

## ■ REFERENCES


(1) Ambartsumyan, R. V.; Basov, N. G.; Kryukov, P. G.; Letokhov, V. S. 5A10 (B)-a Laser with a Nonresonant Feedback. *IEEE J. Quantum Electron.* **1966**, *2*, 442−446.

(2) Letokhov, V. S. Generation of Light by a Scattering Medium with Negative Resonance Absorption. *Sov. Phys. J. Exp. Theor. Phys.* **1967**, *53*, 1442−1452.

(3) Lawandy, N. M.; Balachandran, R. M.; Gomes, A. S. L.; Sauvain, E. Laser Action in Strongly Scattering Media. *Nature* **1994**, *368*, 436−438.

(4) Balachandran, R. M.; Pacheco, D. P.; Lawandy, N. M. Laser Action in Polymeric Gain Media Containing Scattering Particles. *Appl. Opt.* **1996**, *35*, 640−643.

(5) Cao, H.; Zhao, Y. G.; Ho, S. T.; Seelig, E. W.; Wang, Q. H.; Chang, R. P. H. Random Laser Action in Semiconductor Powder. *Phys. Rev. Lett.* **1999**, *82*, 2278.

(6) Frolov, S. V.; Vardeny, Z. V.; Yoshino, K.; Zakhidov, A.; Baughman, R. H. Stimulated Emission in High-Gain Organic Media. *Phys. Rev. B: Condens. Matter Mater. Phys.* **1999**, *59*, R5284.

(7) Cao, H.; Xu, J. Y.; Chang, S.-H.; Ho, S. T. Transition from Amplified Spontaneous Emission to Laser Action in Strongly Scattering Media. *Phys. Rev. E: Stat. Phys., Plasmas, Fluids, Relat. Interdiscip. Top.* **2000**, *61*, 1985−1989.

(8) Cao, H. Review on Latest Developments in Random Lasers with Coherent Feedback. *J. Phys. A: Math. Gen.* **2005**, *38*, 10497.

(9) Wiersma, D. S. The Physics and Applications of Random Lasers. *Nat. Phys.* **2008**, *4*, 359−367.

(10) Jiang, X.; Soukoulis, C. M. Time Dependent Theory for Random Lasers. *Phys. Rev. Lett.* **2000**, *85*, 70−73.

(11) Apalkov, V. M.; Raikh, M. E.; Shapiro, B. Random Resonators and Prelocalized Modes in Disordered Dielectric Films. *Phys. Rev. Lett.* **2002**, *89*, 16802.

(12) Vanneste, C.; Sebbah, P.; Cao, H. Lasing with Resonant Feedback in Weakly Scattering Random Systems. *Phys. Rev. Lett.* **2007**, *98*, 143902.

(13) Polson, R. C.; Vardeny, Z. V. Random Lasing in Human Tissues. *Appl. Phys. Lett.* **2004**, *85*, 1289.

(14) Polson, R. C.; Vardeny, Z. V. Cancerous Tissue Mapping from Random Lasing Emission Spectra. *J. Opt.* **2010**, *12*, 24010.

(15) Song, Q.; Xiao, S.; Xu, Z.; Liu, J.; Sun, X.; Drachev, V.; Shalaev, V. M.; Akkus, O.; Kim, Y. L. Random Lasing in Bone Tissue. *Opt. Lett.* **2010**, *35*, 1425.

(16) Smuk, A.; Lazaro, E.; Olson, L. P.; Lawandy, N. M. Random Laser Action in Bovine Semen. *Opt. Commun.* **2011**, *284*, 1257−1258.

(17) Gottardo, S.; Cavalieri, S.; Yaroshchuk, O.; Wiersma, D. S. Quasi-Two-Dimensional Diffusive Random Laser Action. *Phys. Rev. Lett.* **2004**, *93*, 263901.

(18) Kreibig, U.; Vollmer, M. *Optical Properties of Metal Clusters*; Springer: Berlin, Germany, 1995.

(19) Meng, X.; Fujita, K.; Murai, S.; Tanaka, K. Coherent Random Lasers in Weakly Scattering Polymer Films Containing Silver Nanoparticles. *Phys. Rev. A: At., Mol., Opt. Phys.* **2009**, *79*, 53817.

(20) Dominguez, C. T.; Maltez, R. L.; dos Reis, R. M. S.; de Melo, L. S. A.; de Araújo, C. B.; Gomes, A. S. L. Dependence of Random Laser Emission on Silver Nanoparticle Density in PMMA Films Containing Rhodamine 6G. *J. Opt. Soc. Am. B* **2011**, *28*, 1118.

(21) Maier, S. A. *Plasmonics: Fundamentals and Applications*; Springer: New York, 2007.

(22) Ziegler, J.; Djiango, M.; Vidal, C.; Hrelescu, C.; Klar, T. A. Gold Nanostars for Random Lasing Enhancement. *Opt. Express* **2015**, *23*, 15152.

(23) Nehl, C. L.; Liao, H.; Hafner, J. H. Optical Properties of Star-Shaped Gold Nanoparticles. *Nano Lett.* **2006**, *6*, 683−688.

(24) Hao, F.; Nehl, C. L.; Hafner, J. H.; Nordlander, P. Plasmon Resonances of a Gold Nanostar. *Nano Lett.* **2007**, *7*, 729−732.

(25) Khoury, C. G.; Vo-Dinh, T. Gold Nanostars for Surface-Enhanced Raman Scattering: Synthesis, Characterization and Optimization. *J. Phys. Chem. C* **2008**, *112*, 18849−18859.

(26) Hrelescu, C.; Sau, T. K.; Rogach, A. L.; Jaeckel, F.; Laurent, G.; Douillard, L.; Charra, F. Selective Excitation of Individual Plasmonic Hotspots at the Tips of Single Gold Nanostars. *Nano Lett.* **2011**, *11*, 402−407.

(27) Dice, G. D.; Mujumdar, S.; Elezzabi, A. Y. Plasmonically Enhanced Diffusive and Subdiffusive Metal Nanoparticle-Dye Random Laser. *Appl. Phys. Lett.* **2005**, *86*, 131105.
(28) Meng, X.; Fujita, K.; Zong, Y.; Murai, S.; Tanaka, K. Random Lasers with Coherent Feedback from Highly Transparent Polymer Films Embedded with Silver Nanoparticles. *Appl. Phys. Lett.* **2008**, *92*, 201112.
(29) Meng, X.; Fujita, K.; Murai, S.; Matoba, T.; Tanaka, K. Plasmonically Controlled Lasing Resonance with Metallic−Dielectric Core−Shell Nanoparticles. *Nano Lett.* **2011**, *11*, 1374−1378.
(30) Zhai, T.; Zhang, X.; Pang, Z.; Su, X.; Liu, H.; Feng, S.; Wang, L. Random Laser Based on Waveguided Plasmonic Gain Channels. *Nano Lett.* **2011**, *11*, 4295−4298.
(31) Heydari, E.; Flehr, R.; Stumpe, J. Influence of Spacer Layer on Enhancement of Nanoplasmon-Assisted Random Lasing. *Appl. Phys. Lett.* **2013**, *102*, 133110.
(32) Zhai, T.; Chen, J.; Chen, L.; Wang, J.; Wang, L.; Liu, D.; Li, S.; Liu, H.; Zhang, X. A Plasmonic Random Laser Tunable through Stretching Silver Nanowires Embedded in a Flexible Substrate. *Nanoscale* **2015**, *7*, 2235−2240.
(33) Ning, S.; Wu, Z.; Dong, H.; Ma, L.; Jiao, B.; Ding, L.; Ding, L.; Zhang, F. The Enhanced Random Lasing from Dye-Doped Polymer Films with Different-Sized Silver Nanoparticles. *Org. Electron.* **2016**, *30*, 165−170.
(34) Munkhbat, B.; Pöhl, H.; Denk, P.; Klar, T. A.; Scharber, M. C.; Hrelescu, C. Performance Boost of Organic Light-Emitting Diodes with Plasmonic Nanostars. *Adv. Opt. Mater.* **2016**, *4*, 772−781.
(35) Jana, N. R.; Gearheart, L.; Murphy, C. J. Wet Chemical Synthesis of High Aspect Ratio Cylindrical Gold Nanorods. *J. Phys. Chem. B* **2001**, *105*, 4065−4067.
(36) Fales, A. M.; Yuan, H.; Vo-Dinh, T. Development of Hybrid Silver-Coated Gold Nanostars for Non-Aggregated Surface-Enhanced Raman Scattering. *J. Phys. Chem. C* **2014**, *118*, 3708−3715.
(37) Fales, A. M.; Yuan, H.; Vo-Dinh, T. Silica-Coated Gold Nanostars for Combined Surface-Enhanced Raman Scattering (SERS) Detection and Singlet-Oxygen Generation: A Potential Nanoplatform for Theranostics. *Langmuir* **2011**, *27*, 12186−12190.
(38) Shaklee, K. L. Direct Determination of Optical Gain in Semiconductor Crystals. *Appl. Phys. Lett.* **1971**, *18*, 475.
(39) Link, S.; Wang, Z. L.; El-Sayed, M. A. Alloy Formation of Gold−Silver Nanoparticles and the Dependence of the Plasmon Absorption on Their Composition. *J. Phys. Chem. B* **1999**, *103*, 3529−3533.
(40) Meng, X.; Fujita, K.; Moriguchi, Y.; Zong, Y.; Tanaka, K. Metal-Dielectric Core-Shell Nanoparticles: Advanced Plasmonic Architectures Towards Multiple Control of Random Lasers. *Adv. Opt. Mater.* **2013**, *1*, 573−580.
(41) Brackmann, U. *Lambdachrome Laser Dyes: Data Sheets*; Lambda Physik: Göttingen, Germany, 2000.
(42) Zhang, M.; Rene-Boisneuf, L.; Hu, Y.; Moozeh, K.; Hassan, Y.; Scholes, G.; Winnik, M. A. Preparation and Photo/chemical-Activation of Wormlike Network Micelles of Core−shell Quantum Dots and Block Copolymer Hybrids. *J. Mater. Chem.* **2011**, *21*, 9692.



DOI: 10.1021/acs.jpcc.6b05737
*J. Phys. Chem. C* 2016, 120, 23707−23715